Estimation of Evapotranspiration Using a Nonparametric Approach Under All Sky: Accuracy Evaluation and Error Ana....

Article *in* IEEE Journal of Selected Topics in Applied Earth Observations and Remote Sensing · June 2017

DOI: 10.1109/JSTARS.2017.2707586

5 authors, including:

Xin Pan
Hohai University
10 PUBLICATIONS **18** CITATIONS
SEE PROFILE

Yuanbo Liu
Chinese Academy of Sciences
70 PUBLICATIONS **1,002** CITATIONS
SEE PROFILE

Xingwang Fan
Chinese Academy of Sciences
27 PUBLICATIONS **63** CITATIONS
SEE PROFILE

Estimation of Evapotranspiration Using a Nonparametric Approach Under All Sky: Accuracy Evaluation and Error Analysis

Xin Pan, Yuanbo Liu, Guojing Gan, Xingwang Fan, and Yingbao Yang

***Abstract*—Accurate estimation of regional evapotranspiration (ET) or latent heat flux (latent energy, LE) remains a challenge. On the basis of a nonparametric approach, this study proposed an all-sky algorithm based on moderate-resolution imaging spectroradiometer (MODIS) products and datasets of China Meteorological Administration Land Data Assimilation System (CLDAS). Eddy covariance observations from three nonvegetated sites (desert, Gobi, and village) and three vegetated sites (orchard, vegetable, and wetland) over an arid/semiarid region were used as references to validate the new algorithm. Results showed that the spatial and temporal patterns of LE coincided with desert–oasis ecosystems. Comparison of the retrieved and reference values yielded the following results: R^2 = 0.19–0.63, bias = −129–56 W/m^2, relative error (RE) = 5%–29%, and root-mean-square error (RMSE) = 95–150 W/m^2. Remote-sensing-retrieved LE (RSLE) exhibited relatively good accuracy and poor agreement with ground observations at the nonvegetated sites (RE: 5%–23%, R^2: 0.19–0.40), whereas contradicting scenario occurred at the vegetated sites (RE: 24%–29%, R^2: 0.46–0.63). In the arid nonvegetated region, the ET error might have been caused by net radiation, soil heat flux, land surface temperature, and air temperature. In the vegetated region, the errors of MODIS and CLDAS products were not the dominant error sources of RSLE. The validation supported the applicability of the proposed algorithm in the arid/semiarid region.**

***Index Terms*—All sky, eddy covariance (EC), evapotranspiration (ET), nonparametric (NP) approach, remote sensing retrieval.**

Nomenclature

The table of all acronyms is listed as follow:

ERLE	Energy balance corrected LE
$G_{\rm s}$	Soil heat flux
$H_{\rm s}$	Sensible heat flux
LE	Latent heat flux (Evapotranspiration)
MODLE	Retrieved LE in clear-sky approach
NDVI	Normalized difference vegetation index
P	Near-surface pressure
q	Relative humidity
$R_{\rm ld}$	Downwelling longwave radiation
$R_{\rm lu}$	Upwelling longwave radiation
R_n	Net radiation
$R_{\rm sd}$	Downwelling shortwave radiation
RSLE	Retrieved LE in all-sky approach
T_a	Near-surface air temperature
T_c	Cloud temperature
T_s	Land surface temperature
α	Albedo
Δ	Slope of the saturated vapor pressure at T_a
ε_C	Cloud emissivity
ε_S	Land surface emissivity

Manuscript received September 12, 2016; revised January 2, 2017, March 16, 2017, and April 12, 2017; accepted May 19, 2017. Date of publication June 5, 2017; date of current version July 17, 2017. This work was supported in part by the National Natural Science Foundation of China (91125004), in part by the China Postdoctoral Science Foundation Funded Project (2017M611665), in part by the Key Project of Water Resources Department of Jiangxi Province (KT201506), and in part by the Fundamental Research Funds for the Central Universities of China by the project funded by the Priority Academic Program Development of Jiangsu Higher Education Institution. *(Corresponding author: Yuanbo Liu.)*

X. Pan and Y. Yang is with School of Earth Science and Engineering, Hohai University, Nanjing 210098, China (e-mail: px1013@163.com; yyb@hhu.edu.cn).

Y. Liu, G. Gan, and X. Fan are with Key Laboratory of Watershed Geographic Sciences, Nanjing Institute of Geography and Limnology, Chinese Academy of Sciences, Nanjing 210008, China (e-mail: ybliu@niglas.ac.cn; gjgan@niglas.ac.cn; xwfan1989@163.com).

Color versions of one or more of the figures in this paper are available online at http://ieeexplore.ieee.org.

Digital Object Identifier 10.1109/JSTARS.2017.2707586

I. Introduction

EVAPOTRANSPIRATION (ET) is the sum of evaporation from soil surfaces and transpirations from plant tissues. ET controls the water/energy transport in the biosphere, atmosphere, and hydrosphere, and it is vital in evaluating regional water resources, especially in arid regions [1]. Latent energy (LE), a vital component of the surface energy balance, is consumed during ET. Accurate estimation of the ET flux is critical, especially at large spatiotemporal scales. Ground-based measuring devices can observe ET with satisfactory accuracy. Such devices include lysimeters, eddy covariance (EC) systems, and Bowen ratio systems [2]–[4]. Nevertheless, point-scale measurements cannot always accurately represent trends over large areas, and densely distributed sites are not feasible [5]. Alternatively, remote sensing provides a viable method for monitoring ET. Penman [6] first studied ET, and since then, many methods and algorithms that combine remote-sensing observations with ancillary surface and atmosphere data have been proposed for ET estimation; these methods include the triangle approach, surface energy balance system (SEBS), MOD16 algorithm, three-temperature model, and two-source energy balance (TSEB) model [7]–[15].

These methods have been successfully applied for regional and global ET estimations. For example, Knipper et al. [7] used moderate-resolution imaging spectroradiometer (MODIS)

products and the triangle approach to retrieve LE in a semiarid region covered with evergreen forest and shrubs, with a relative error (RE) of 24%–32%. Su *et al*. [8] used MODIS data and the SEBS model to assess LE in wheat, corn, and rainforest areas, with an RE of 25%. Ma *et al*. [9] also retrieved LE that was based on the revised SEBS model and advanced spaceborne thermal emission and reflection radiometer (ASTER) images and obtained an overall RE of 15% in cropland, residential, orchard, Gobi, sandy desert, desert steppe, and wetland areas. Mu *et al*. [10] used MODIS products, meteorological auxiliary data, and MOD16 algorithm to produce MOD16 products and reported an RE of 24% for daily ET. Xiong and Qiu [11] estimated LE in grasslands and hills through the three-temperature approach and Landsat Thematic Mapper data. Their study yielded an RE of 5%–100% during the satellite overpass time. Song *et al*. [12] improved the TSEB and validated its reliability in the Heihe Basin. Similarly, Dhungel *et al*. [13] presented physical based two source surface energy balance model (TSEB) using NARR (North American Reanalysis Data) and Landsat data in 3-h temporal resolution to capture role of the irrigation and precipitation between the satellite overpass, which can be critical in agricultural dominant areas. Although these methods have presented relatively high accuracies, their accuracies cannot be significantly improved easily due to the daunting validations of resistance parameterization or empirical coefficient. The complexity and nonuniqueness of resistance parameterization also limits these methods [10], [16].

Nonparametric (NP) ET approach offers a simple and analytical method for LE estimation [17]. Relative to other approaches to LE estimation, a few inputs of NP approach, including the net radiation (R_n), surface air temperature, land surface temperature, and soil heat flux (G_s), exist and are measurable. Furthermore, the NP approach does not require resistance parameterization or empirical coefficient, and thus, exhibits considerable potential in LE estimation. The LE estimated through NP approach and based on ground meteorological data has been validated at the point scale at 24 sites and yielded a satisfactory accuracy and a bias of 10.3 ± 20.2 W/m^2 [17]. Instantaneous LE has been retrieved under clear sky on the basis of MODIS products and the NP approach; the obtained RE in a semiarid region is 9%–48% [18]. However, cloudy or overcast days also occur during a long period. The phenomenon under a clear sky differs significantly from that under a cloudy sky. Thus, this study estimated and evaluated instantaneous LE under all sky through a new algorithm based on the NP approach to estimate LE at long time scales. The remainder of this paper is organized as follows: Section II introduces the algorithm. Section III presents the selected sites and required data. Section IV reveals and validates the results and analyzes the error sources, and Section V concludes this study.

II. Methodology

A. Methods of R_n and G_s Retrieval

R_n can be expressed in terms of its components as follows:

$$R_n = (1-\alpha)\, R_{sd} + R_{ld} - R_{lu} \tag{1}$$

where R_{sd} is the downwelling shortwave radiation, R_{ld} is the downwelling longwave radiation, R_{lu} is the upwelling longwave radiation, and α is the surface albedo. R_{sd} can be directly obtained from the China Meteorological Administration Land Data Assimilation System (CLDAS) datasets. Albedo can be obtained from the following equation [19]: $\alpha = 0.160\alpha_1 + 0.291\alpha_2 + 0.243\alpha_3 + 0.116\alpha_4 + 0.112\alpha_5 + 0.081\alpha_7$, where α_1, α_2, α_3, α_4, α_5, and α_7 are the nadir bidirectional Reflectance Distribution Function (BRDF)-adjusted albedos in bands 1, 2, 3, 4, 5, and 7 of MODIS, respectively.

Stefan–Boltzmann equation was used to determine the upward longwave radiation as follows [20], [21]:

$$R_{lu} = \sigma \varepsilon_s T_s^4 \tag{2}$$

where σ is the Stefan–Boltzmann constant (5.67×10^{-8} W/m^2·K^4), T_s is the land surface temperature, and ε_s is the surface emissivity. When the sky is clear, the surface temperature can be obtained from MYD11. However, when the sky is cloudy, the surface temperature can be obtained from MYD06 [22], [23]. In addition, under clear sky, ε_s can be expressed as follows: $\varepsilon_s = 0.273 + 1.778\varepsilon_{31} - 1.807\varepsilon_{31}\varepsilon_{32} - 1.037\varepsilon_{32} + 1.774\varepsilon_{32}^2$, where ε_{31} and ε_{32} denote the emissivity in bands 31 and 32 of MODIS, respectively [19]. The surface emissivity under cloudy sky was obtained from the surface emissivity under clear sky closest to the retrieval moment.

The downward longwave radiation was calculated using the following relationship [24]:

$$R_{ld} = \sigma \varepsilon_a T_a^4 + (1-\varepsilon_a)\sigma \varepsilon_c T_c^4 \tag{3}$$

where T_a is the air temperature obtained from CLDAS, ε_a is the atmospheric emissivity, T_c is the cloud temperature obtained from MYD06, and ε_c is the cloud emissivity obtained from MYD06. The atmospheric emissivity can be estimated using the following equation [25]:

$$\varepsilon_a = \left[1 - \left(1 + \frac{46.5 e_0}{T_a}\right) \exp\left\{-\left(1.2 + 3 \cdot \frac{46.5 e_0}{T_a}\right)^{1/2}\right\}\right] \tag{4}$$

where e_0 is the near-surface water vapor pressure, which can be expressed as follows: $e_0 = p/[1 + 0.628/(q - 1)]$, where p is the near-surface pressure, and q is the relative humidity. p, q, and T_a are all derived from CLDAS.

G_s is parameterized using the normalized difference vegetation index (NDVI) and R_n [26].

$$G_s = 0.583 \exp(-2.13\mathrm{NDVI})\, R_n. \tag{5}$$

B. LE Estimation Using the NP Approach

R_n is transformed into G_s, LE, and sensible heat flux (H_s). Assuming that a homogeneous terrestrial ground surface layer is a macrostate system, R_n is the potential energy, and G_s, H_s, and LE are the kinetic energy. Therefore, the total energy (potential energy + kinetic energy) of this system is Hamiltonian, and the NP approach can be used to calculate the partial differential equations of the Hamiltonian system based on the land surface

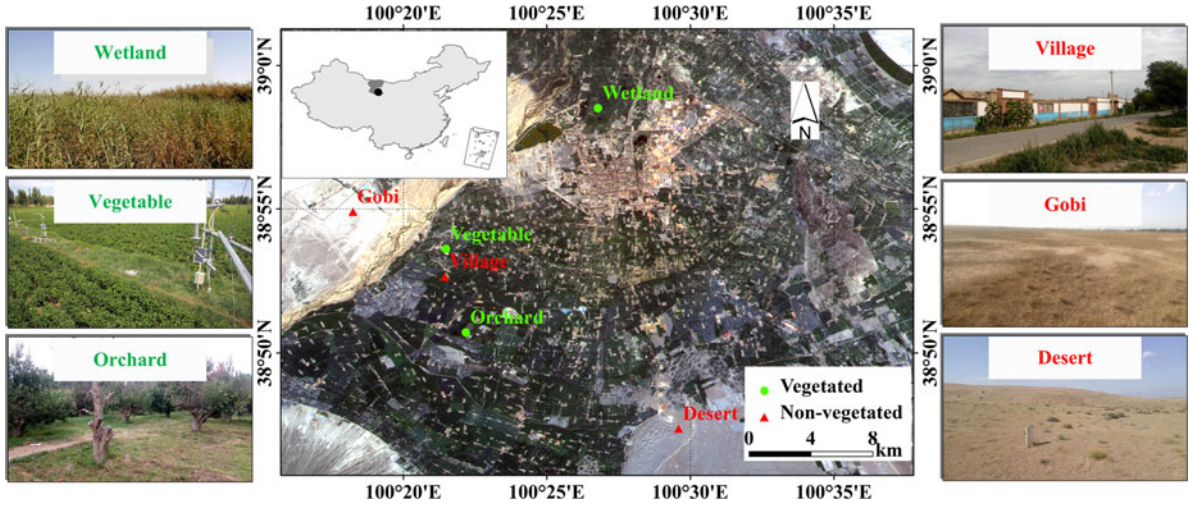

Fig. 1. Site distribution and site surfaces.

temperature. LE is given as follows [17]:

$$LE_{T_s} = \frac{\Delta}{\Delta+\gamma}(R_n - G_s) - \varepsilon_s \sigma \left(T_s^4 - T_a^4\right) + G_s \ln\left(\frac{T_s}{T_a}\right) \tag{6}$$

where γ is the psychometric constant, and Δ is the slope of the saturated vapor pressure at temperature T_a. Δ can be estimated as follows [27], [28]:

$$\Delta = \frac{4098 \cdot \left[0.6108 \cdot \exp\left\{\frac{17.27 \cdot (T_a - 273.15)}{T_a - 35.85}\right\}\right]}{(T_a - 35.85)^2}. \tag{7}$$

C. Correction Approaches for EC Measurements

Although EC techniques can measure LE and H_s with satisfactory accuracy, surface energy imbalance often occurs with a closure of the energy balance of approximately 80% [29]. One of the correction methods can be obtained from the energy balance [30]. On a large-scale homogeneous surface, the corrected LE (ERLE) can be expressed as follows:

$$\mathrm{ERLE} = R_n - G_s - H_{\mathrm{EC}} \tag{8}$$

where H_{EC} is the H_s measured by EC. The ERLE is a reference that validates LE retrieval. Regardless of the influences of ice melt, biomass storage, and advection, this equation is reliable in nonforested regions [31].

D. Quantification of Error Sources for LE Retrieval

The error associated with LE retrieval includes errors in input data and the NP approach. To clarify and quantify the error sources, the error contributions of retrieval errors with respect to each error source should be calculated using error source analysis [18].

The remote sensing-retrieved LE (RSLE) errors were derived from the discrepancies between RSLE and ERLE. The error contribution of each input parameter was calculated based on the parameter derived from MODIS/CLDAS and all actual parameters measured by automatic weather stations (AWSs). Moreover, the error associated with the NP approach was estimated according to the discrepancies between ERLE and LE calculations using the NP approach and all actual parameters.

E. Metrics for Accuracy Assessment

In this study, the coefficient of determination (R^2) of the linear fit between RSLE and ERLE was used to evaluate the agreement and can be described as follows [32]:

$$R^2 = 1 - \frac{\sum_{i=1}^{n}(s_i - o_i)^2}{\sum_{i=1}^{n}(s_i - \bar{o})^2} \tag{9}$$

where s_i is a retrieved value; o_i is a reference value; $\bar{o}$ is the average of o_i, where $i = 1, \ldots, n$; and n is the number of values being compared. R^2 is near 1.0, and the agreement between estimations and references is good.

Bias, RE, and root mean square error (RMSE) were introduced to evaluate the discrepancies in RSLE and ERLE, and they can be described as follows [33].

$$\mathrm{Bias} = \frac{\sum_{i=1}^{n}(s_i - o_i)}{n} \tag{10}$$

$$\mathrm{RE} = \frac{|\mathrm{Bias}|}{\frac{1}{n}\sum_{i=1}^{n} o_i} \times 100\% \tag{11}$$

$$\mathrm{RMSE} = \sqrt{\frac{\sum_{i=1}^{n}(s_i - o_i)^2}{n}}. \tag{12}$$

These three metrics represent different properties of RSLE errors. In detail, bias quantifies the average absolute difference between RSLE and ERLE. RE is the absolute value of the bias divided by the average of ERLE. RMSE reveals a combination of the standard deviation and bias.

III. Study Area and Data Description

A. Study Area and Ground Sites

The study area is located at the Heihe Basin, which is the second largest inland river basin in the northwestern arid/semiarid region of China. This basin possesses a continental climate with

TABLE I
DESCRIPTIVE INFORMATION FOR EC SITES

Type	Site	Latitude (°)	Longitude (°)	Elevation (m)	EC Height (m)
Vegetated	Wetland	38.975	100.446	1 460	5.2
	Vegetable	38.893	100.358	1 552	3.8
	Orchard	38.845	100.370	1 559	7.0
Non-vegetated	Village	38.878	100.358	1 561	4.2
	Gobi	38.915	100.304	1 562	4.6
	Desert	38.789	100.493	1 594	4.6

an annual mean air temperature of 7.4 °C, a multiyear mean of annual precipitation of 115.6 mm, and an average annual evaporation of 2107.1 mm. In our study, six sites were selected in the middle reaches of the Heihe Basin (97°24′ E–102°10′ E, 37°41′–42°42′ N) [34] (see Fig. 1). They belonged to the Heihe Watershed Allied Telemetry Experimental Research (HiWATER) project, which is a comprehensive experiment involving biological, meteorological, and hydrological studies in the typical arid/semiarid region [35], [36]. At all selected sites, LE and H_s were measured by EC systems, and the near-surface meteorological parameters were measured using AWSs. R_n and G_s were measured by pyrgeometers/pyranometers and heat flux plates, respectively. For representativeness, the selected sites were mainly located on different surfaces, including moist vegetated areas (vegetable, orchard, and wetland areas) and arid, nonvegetated areas (village, desert, and Gobi areas). For convenience, the site names were replaced with the types of underlying surfaces. Table I shows the longitude, latitude, elevation, EC height, and land cover of each site.

All instruments were inter-compared in the Gobi between May 14 and 24, 2012 [37]. The intercompared instruments, which exhibited good agreement, ensured the reliability of data.

B. Data Description

The data used for ET retrieval were obtained from MODIS and CLDAS products. MODIS products were provided by the Level 1 and Atmosphere Archive and Distribution System (LAADS) of the National Aeronautics and Space Administration (NASA) in the standard hierarchical data format [38]. In our study, MYD06, MYD11, MYD13, and MCD43 were selected to obtain the retrieved LE (RSLE). The instantaneous values of cloud temperature, cloud emissivity, and T_s (under cloudy sky) were obtained from MYD06, and the instantaneous values of T_s and $\varepsilon_{\rm s}$ under clear sky were obtained from MYD11 [39]–[41]. MYD13 provided 16-day NDVI, and MCD43 provided 8-day nadir BRDF-adjusted albedo, including the albedo in bands 1–7 of MODIS [42]–[44]. CLDAS is a land surface data assimilation product provided by the National Meteorological Information Center of China [45], [46]. In our study, CLDAS provided the air temperature, pressure, relative humidity, and surface downwelling shortwave radiation.

ASTER radiometer possesses five thermal infrared (TIR) bands that provide TIR spectral emissivity variations at a 90-m spatial resolution [47]. The $\varepsilon_{\rm s}$ product is produced by the temperature and emissivity separation algorithm [48]. In our study, the ASTER product was provided by the Cold and Arid Regions Science Data Center at Lanzhou [49], [50]. $\varepsilon_{\rm s}$ can be represented by the ASTER narrowband emissivities using the following linear equation [51]:

$$\varepsilon_s = 0.197 + 0.025\varepsilon_{10} + 0.057\varepsilon_{11} + 0.237\varepsilon_{12} + 0.333\varepsilon_{13} + 0.146\varepsilon_{14} \tag{13}$$

where $\varepsilon_{10} - \varepsilon_{14}$ are the five ASTER narrowband emissivities, which were regarded as the real values of $\varepsilon_{\rm s}$ because of their high accuracies and spatial resolutions. On the basis of a stable surface emissivity over a period of time, the actual surface broadband emissivity can be represented by the ASTER narrowband emissivities.

TABLE II
DATASETS USED IN THE ANALYSIS

Dataset	Parameters	Temporal–Spatial Resolution	Data Type	Data Purpose
EC	LE/H_s	30 min, Hundreds of meters	Meteorology	Validation
AWS	$P/R_{\rm ld}/R_{\rm lu}/T_a/R_n/G_s$	10 min, Several meters to hundreds of meters	Meteorology	Validation
ASTER	$\varepsilon_{\rm s}$	10–20 days, 90 m	Remote Sensing	Validation
CLDAS	$P/T_{\rm a}$ /q/$R_{\rm sd}$	Hourly, 1/16°	Remote Sensing	Retrieval
MYD06	$T_c/\varepsilon_c/T_s$	Instantaneous, 1 km	Remote Sensing	Retrieval
MCD43	α	8 days, 1 km	Remote Sensing	Retrieval
MYD11	$T_s/\varepsilon_{\rm s}$	Instantaneous, 1 km	Remote Sensing	Retrieval
MYD13	NDVI	16 days, 1 km	Remote Sensing	Retrieval

For these products, the pixels located at the sites were used to retrieve and validate LE. All selected images were acquired between 13:00 and 15:00 (local time) from June 25, 2012 to September 15, 2012. The temporal and spatial resolutions of these products are listed in Table II.

Accordingly, the EC and AWS data spanned from June 25, 2012 to September 15, 2012. All AWS and EC data were also provided by the Cold and Arid Regions Science Data Center at Lanzhou [37], [52], [53]. They were used for validation and error source analysis of RSLE. During this period, the average energy balance closure ratio of these data was 0.92 [54]. ERLE, which provides the reference for RSLE, was obtained from the H_s measured by EC and from R_n and G_s measured by AWS to close the energy balance (7).

For the flux data, the raw 10-Hz EC data were corrected for spike detection, lag correction of H_2O relative to the vertical wind component, sonic virtual temperature correction, coordinating rotation, correction for density fluctuation, frequency response correction, and so on. High-quality data were selected to upscale to 30-min flux data. The parameters derived from AWS with a temporal resolution of 10 min were averaged to obtain mean in 30 min, and thereby, match the temporal resolution of EC [55].

The calculation of LE and H_s through the NP approach requires actual observations of P, T_s, T_a, R_n, and G_s. Excluding T_s, other parameters were measured directly by AWS. The actual T_s was estimated from the upwelling and downwelling longwave radiations measured by AWS through the following

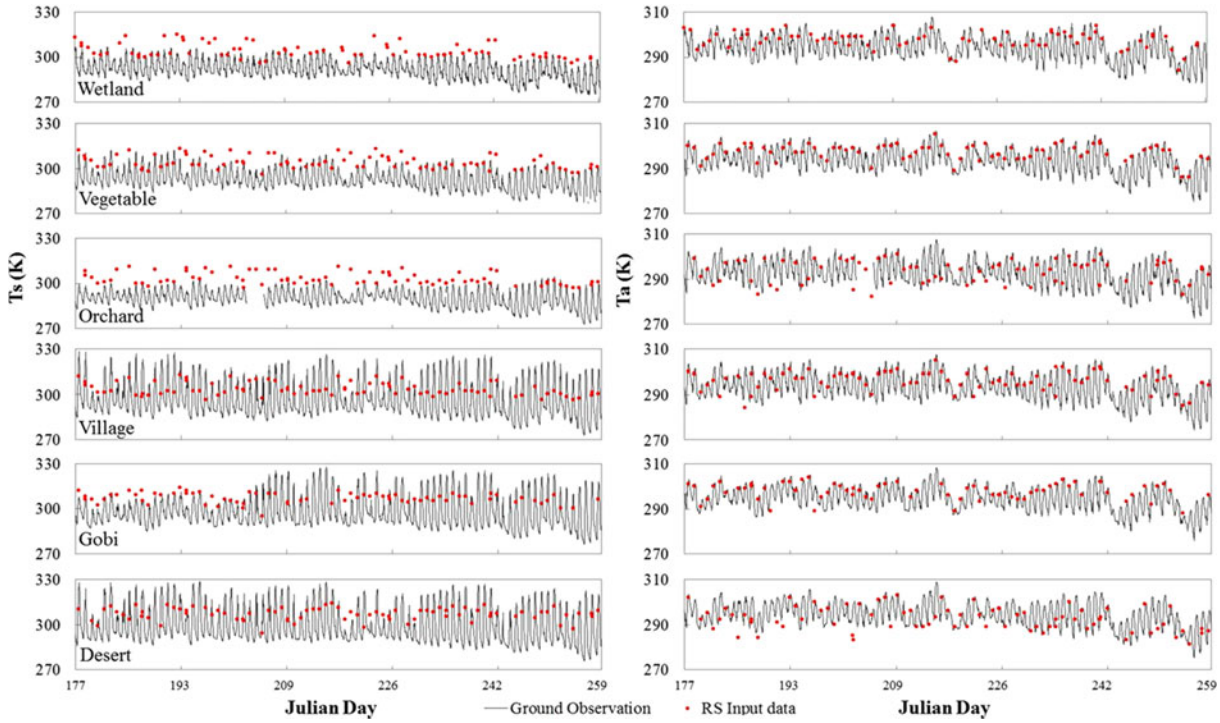

Fig. 2. Temporal variations in T_s and T_a at six selected sites during 25 June–9 September in 2012, including the ground observations at half-hour scale and the instantaneous remote sensing values at the satellite overpass time (13:30, UTC).

equation [49]:

$$T_s = \left[\frac{R_{lu} - (1-\varepsilon_s)\cdot R_{ld}}{\varepsilon_s \cdot \sigma}\right]^{1/4} \tag{14}$$

where ε_s was estimated by the ASTER narrowband emissivities through (10).

The AWS and EC data collected during the satellite overpass time were selected to validate the retrievals.

IV. Results

A. Instantaneous Retrieval Results of R_n, G_s, and LE

During the retrieval period, the ε_s and pressure values were higher at vegetated sites (0.978–0.981 and 84–89 kPa, respectively) than those at nonvegetated sites (0.932–0.975 and 83–84 kPa, respectively). Conversely, T_s ranged from 300 to 305 K at the vegetated sites, while it ranged from 315 to 320 K at the nonvegetated sites (see Fig. 2). The averages of T_a were similar at all sites, with values of approximately 299 K. The T_s derived from MODIS products significantly (insignificantly) agreed with the ground observations under clear (cloudy) sky, especially at the vegetated sites. An agreement was also observed between the T_a derived from CLDAS and the ground observations. This finding provided the background for remote sensing retrieval. According to these environmental parameters, the retrieved R_n was higher at the vegetated sites (508–526 W/m^2) than that at the nonvegetated sites (448–494 W/m^2). The high values of retrieved G_s (approximately 200 W/m^2) were observed at the nonvegetated region because of the low NDVI values. Therefore, the RSLE was higher at the vegetated sites (314–330 W/m^2) than at the nonvegetated sites (150–305 W/m^2).

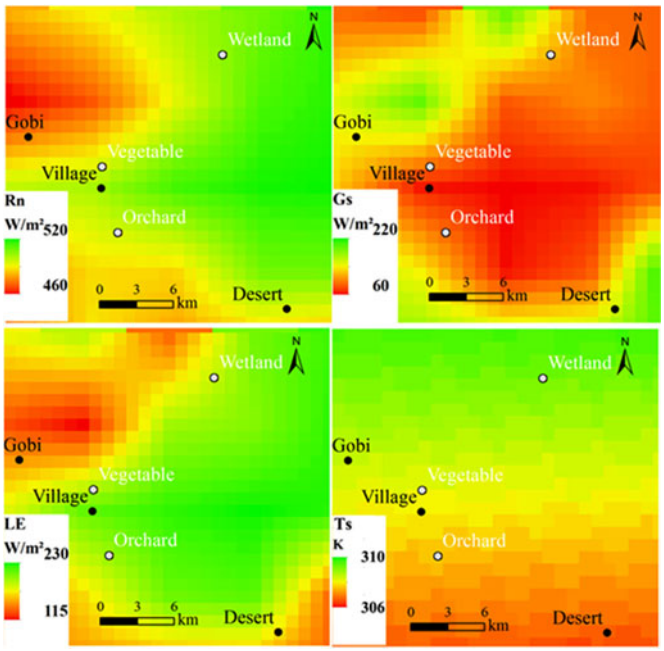

Fig. 3. Distributions of the instantaneous values in the Zhangye Region at 05:55 (UTC) on August 20, 2012, including the retrieved R_n, G_s, LE, and MYD06 T_s.

The instantaneous retrievals of R_n, G_s, and LE with a spatial resolution of 1 km are shown in Fig 3. The distribution of T_s provided by MYD06 is also shown. The distributions matched those of an oasis–desert ecosystem, except for T_s.

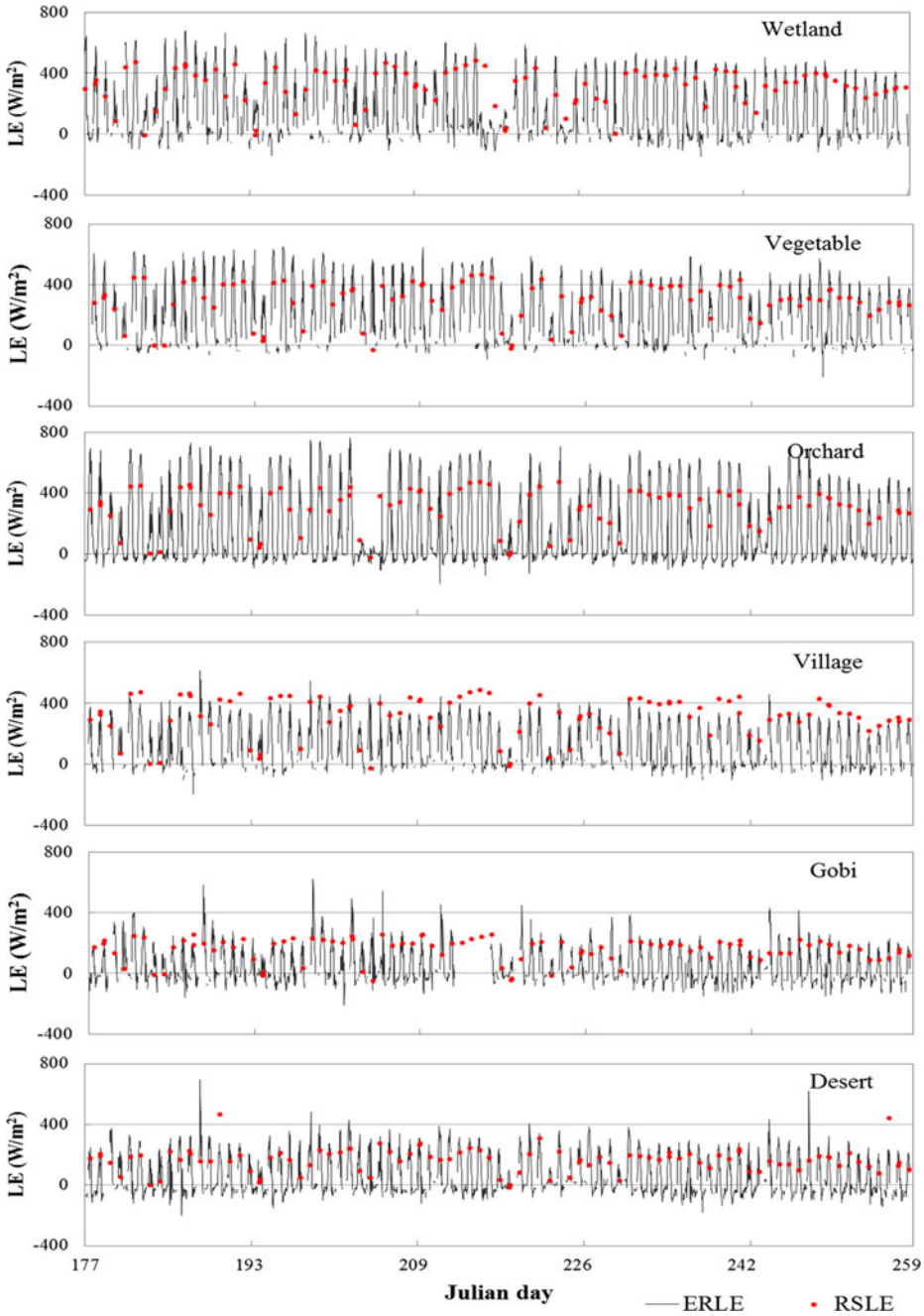

Fig. 4. Temporal variations in LE values at six selected sites during 25 June–9 September in 2012, including the ground observations at half-hour scale and the instantaneous retrieved values at the satellite overpass time (13:30, UTC).

In the desert region, low R_n values were observed because of high albedo, and high G_s values were observed because of bare surfaces. In oasis and wetland areas, considerable LE was observed because of irrigation and inflow to some degree. These results revealed the need of physical-based model, which can capture the precipitation and irrigation through soil water balance in irrigated agriculture areas, which is not incorporated in most of the remote sensing-based ET calculation models [13]. At 05:55 (UTC) on August 20, 2012, RSLE reached 200–250 W/m^2 in the oasis and decreased to 100–150 W/m^2 in the desert.

B. Temporal Variation in Retrieved LE

Fig. 4 shows that ERLE and RSLE temporally varied during 25 June to 9 September in 2012. The RSLE plotted by the red points was based on the instantaneous LE at the satellite overpass time (13:30, UTC). The ERLE plotted by the black line was based on continuous observations at half-hour scale. RSLE can reveal the temporal variation in LE at all sites. Moreover, the RSLE can display the peaks and valleys in temporal variations. The discrepancies between LE under clear sky and LE under cloudy sky can be clearly illustrated. At the vegetated sites, the RSLE was 300–500 W/m^2 under clear sky, and it decreased to

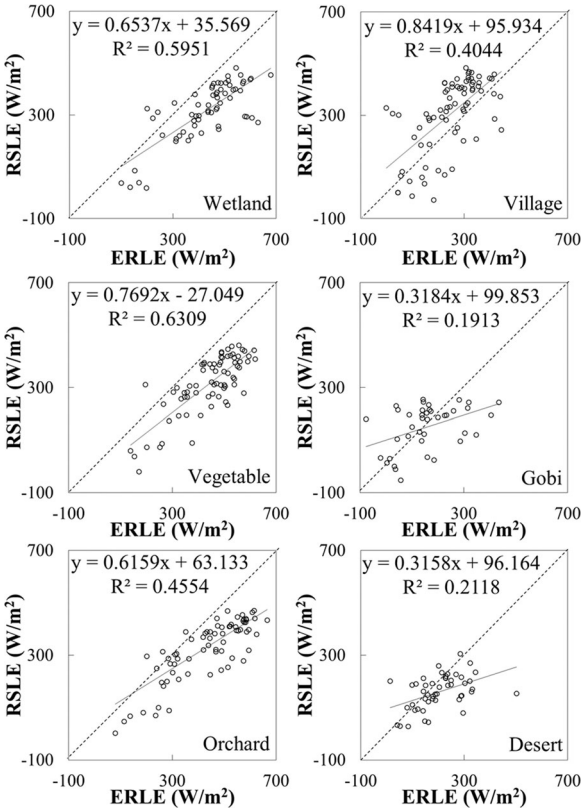

Fig. 5. Comparisons between corrected instantaneous LE (ERLE) and remote sensing-retrieved instantaneous LE (RSLE) at six sites during 25 June–9 September in 2012.

less than 200 W/m^2 under cloudy sky. At the nonvegetated sites, except for village site, the RSLE was 200–300 W/m^2 under clear sky, and it decreased to less than 100 W/m^2 under cloudy sky. The high RSLE of approximately 400 W/m^2 was possibly related to the mixed landscape with a certain amount of trees in the area. Therefore, the RSLE at village site revealed a similar phenomenon relative to the RSLE at vegetated sites at times. The RSLE was considerably underestimated under clear and cloudy skies at vegetated sites, whereas a slight overestimation appeared at nonvegetated sites.

C. Accuracy Assessment of Retrieved LE

Fig. 5 shows the relationship between ERLE and RSLE according to ERLE. In general, the RSLE was relatively accurate, with bias, RMSE, RE, slope, and R^2 values of -59 W/m^2, 133 W/m^2, 18%, 0.56, and 0.48, respectively (see Table III). The accuracy was similar to that of other remote sensing algorithms for LE retrieval [56].

At the site scale, the RSLE was generally underestimated, with R^2 values of 0.19–0.63, bias values of -129–56 W/m^2, RE values of 5%–29%, and RMSE values of 95–150 W/m^2. RSLE had high accuracies at nonvegetated sites (village, Gobi, and desert), but a poor agreement was determined between RSLE and ERLE at these three sites (village, Gobi, and desert). The RE (R^2) values of RSLE ranged from 5% to 23% (0.19–0.40). Conversely, low accuracy and high agreement were observed at

TABLE III
ERRORS OF INSTANTANEOUS RSLE AT SIX SITES AND IN THE OVERALL SITUATION (ALL OBSERVATIONS AT ALL SITES) DURING 25 JUNE–9 SEPTEMBER IN 2012

Statistics	Bias	RMSE	RE	R^2
Units	W/m^2	W/m^2	%	–
Wetland	−114	141	26	0.6
Vegetable	−129	148	29	0.63
Orchard	−103	150	24	0.46
Village	57	123	23	0.4
Gobi	−8	109	5	0.19
Desert	−43	95	21	0.21
Overall	**−59**	**133**	**18**	**0.48**

vegetated sites (wetland, vegetable, and orchard), with RE and R^2 values of 24%–29% and 0.46–0.63, respectively. Therefore, the RSLE exhibited lower systemic error and higher random error at the nonvegetated sites than those at the vegetated sites.

D. Error Sources and Their Contributions to Retrieved LE

The input error of each parameter was first determined to reveal the contributions of the input errors (see Fig. 6). R_n was retrieved with low accuracy at the orchard and three nonvegetated sites (bias values of more than 55 W/m^2). The retrieved G_s exhibited low accuracies at the Gobi and desert sites, with bias values of approximately 170 W/m^2. A large difference (approximately -7 kPa) in surface pressure was observed between wetland and vegetable sites. At most sites, the biases of T_a were less than 1 K. The biases of T_s were 2–6 K at the vegetated sites and ranged from -11 to -5 K at the nonvegetated sites. The ε_s difference between MODIS and ASTER products was less than 0.01 at all sites, except those at the desert site (0.034).

The error contributions can be determined according to the input errors. Fig. 7 shows the error contributions of each factor (shown by the lines) and the RSLE errors (shown by the columns) at six sites. At the vegetated sites, the RSLE was underestimated systematically, and the average bias ranged from -175 to -94 W/m^2. Thus, the RSLE exhibited relatively satisfactory accuracy and large random error (with average biases of -69–69 W/m^2). Error source analysis indicated that the major error sources (inducing an RSLE error of more than 40 W/m^2) were R_n, G_s, T_s, and T_a at the nonvegetated sites, with error contributions of 53–75, -110–4, 21–47, and -49–3 W/m^2, respectively. At the vegetated sites, the input errors were not the dominant error sources of RSLE. The main error source was the error inherent in the NP approach, and the error contribution of the RSLE ranged from -111 to -42 W/m^2. Large G_s error contributions (causing approximately -100 W/m^2 of the RSLE error) were observed at the Gobi and desert sites. More than 50 W/m^2 of the RSLE error caused by the R_n error occurred at the three nonvegetated sites. The influences of T_a and T_s errors on the LE error were below 40 W/m^2 at most sites, except for T_s at the village site, T_a and T_s at the desert site, and T_a at the orchard site. The error contribution of ε_s accounted for a small proportion of the RSLE error (less than 10 W/m^2 of the LE er-

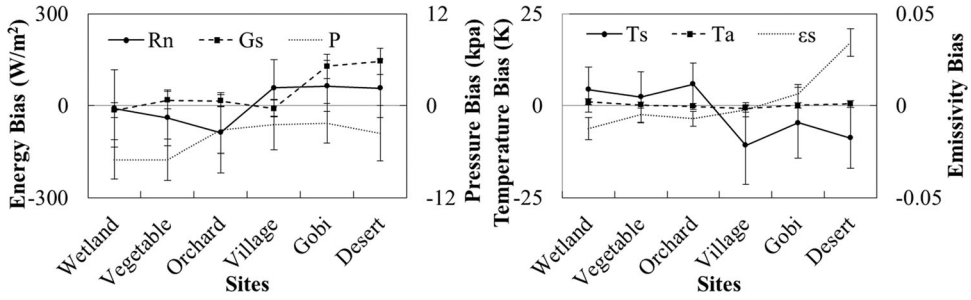

Fig. 6. Averages (lines) and standard deviations (bars) of input parameter errors, including instantaneous values of net radiation (R_n), soil heat flux (G_s), land surface temperature (T_s), near-surface air temperature (T_a), land surface emissivity (ε_s), and near-surface pressure (P), at six sites during 25 June–9 September in 2012.

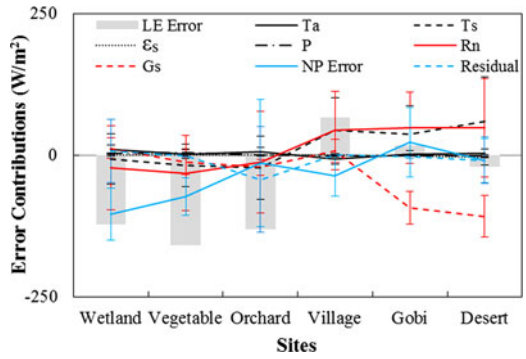

Fig. 7. Error contributions of each factor, including the averages (lines), standard deviations (bars), and RSLE errors (columns) during 25 June–9 September in 2012.

TABLE IV
ERRORS OF THE RETRIEVED INSTANTANEOUS NET RADIATION (R_n _RE) AT SIX SITES DURING 25 JUNE–9 SEPTEMBER IN 2012

Statistics	Bias	RE	RMSE	R^2
Unit	W/m^2	%	W/m^2	–
Wetland	−9	2	127	0.74
Vegetable	−39	7	99	0.74
Orchard	−88	15	158	0.62
Village	58	13	108	0.68
Gobi	64	16	105	0.68
Desert	57	14	111	0.64

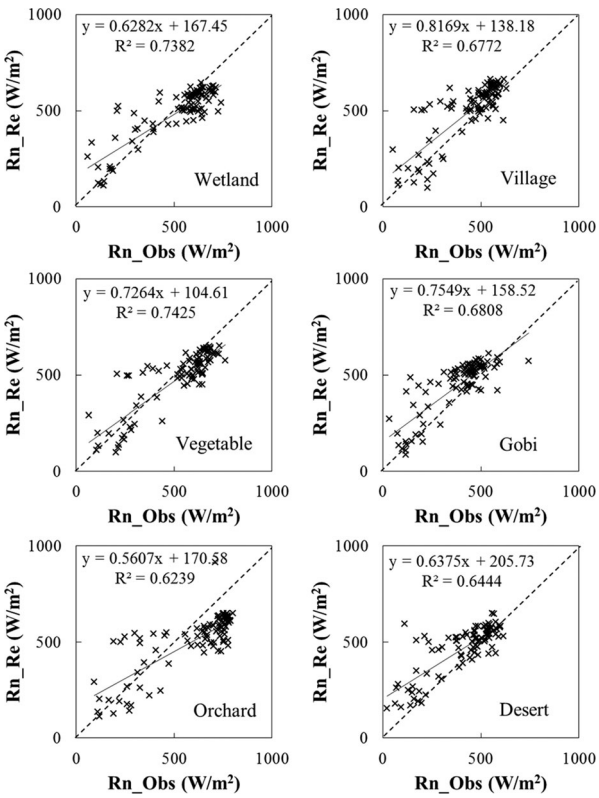

Fig. 8. Comparison of instantaneous net surface radiation observed by the ground instruments (R_n_Obs) and that retrieved by our algorithm (R_n_Re) at six sites during 25 June–9 September in 2012.

ror). Similarly, the pressure input errors minimally affected the RSLE error (generally less than 1 W/m^2).

The scatter diagram is shown in Fig. 8 to further understand the discrepancy of error source about R_n. R_n was underestimated (overestimated) at the vegetated (nonvegetated) sites. Table IV indicates that a large accurate R_n estimation at the vegetated sites, which was accompanied with less RE (2%–15%) and high R^2 (0.62–0.74). By contrast, R_n was estimated unsatisfactorily at the non-vegetated sites with RE (R^2) values of 13%–16% (0.64–0.68). The different error contributions of R_n to RSLE were related to the difference in R_n retrieval accuracy between vegetated and nonvegetated sites. Less (larger) R_n error resulted in less (larger) error contribution of R_n at the vegetated (nonvegetated) sites.

At all sites, R_n was retrieved with relatively poor accuracy when its value was low. This result was probably related to the influence of clouds, which should affect RSLE under cloudy sky.

E. Comparison of All-Sky Algorithm and Previous Clear-Sky Algorithm

The RSLE under all-sky algorithm constituted the RSLE under clear and cloudy skies. In previous research, a satellite retrieval algorithm of clear-sky LE based on NP approach and MODIS products was developed and had significant differences in accuracies at various sites [18]. In this part, under clear sky, RSLE was compared with the LE retrieved by the previous clear-sky MODIS algorithm (MODLE) inFig. 9.

RSLE was evidently more accurate than MODLE at the nonvegetated and orchard sites. In particular, at the Gobi and desert

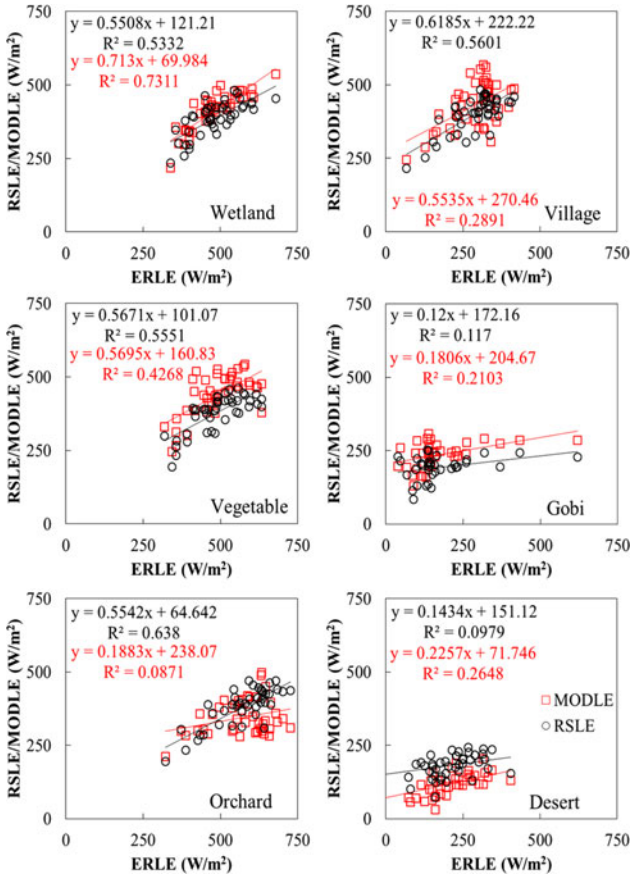

Fig. 9. Comparison among instantaneous LEs observed on the ground (ERLE), LEs retrieved by all-sky algorithm (RSLE), and LEs retrieved by clear-sky algorithm (MODLE) under clear sky during 25 June–9 September in 2012.

sites, the RE of LE decreased from 35%–44% to 10%–13% (see Table V). This decrease indicated that the accuracy of the all-sky algorithm significantly improved relative to the clear-sky algorithm. At the orchard and village sites, compared with MODLE, RSLE also presented a more satisfactory accuracy with a slight RE decrease from 40%–49% to 33%–39% and a remarkable R^2 increase from 0.09–0.29 to 0.56–0.64. Similar accuracy of the retrieved LE was obtained through the clear-sky and all-sky algorithms. The RE and R^2 values were 10%–14% and 0.43–0.73, respectively, for MODLE and 20%–23% and 0.53–0.56, respectively, for RSLE.

The all-sky algorithm in this study generally represented more reliable LE estimation at the three nonvegetated sites and orchard site than the previous clear-sky algorithm, but both algorithms behaved similarly at two other vegetated sites. Therefore, the all-sky algorithm was better than the clear-sky algorithm, especially at the nonvegetated sites, where poor MODLE was obtained.

V. Discussion

LE at a daily or longer temporal scale is urgently required in hydrology, ecology, and agriculture [57], [58]. All-sky LE should be retrieved to obtain continuous daily LE. Only clear-sky LE exhibits difficulty in acquiring the continuous time series of ideal daily LE even after the temporal reconstruction [59]. LE can be estimated every day by using the all-sky algorithm. Accordingly, daily LE can be obtained by instantaneous LE estimation and temporal upscaling approach [22]. The all-sky algorithm of LE estimation in this study, thus, exhibits a wider scope of application than the previous clear-sky algorithm [18].

This study mainly aims to develop an accurate approach based on the NP approach for LE estimation without ancillary ground observations/experiments. In this regard, under clear sky, the LE estimation of the all-sky algorithm is more effective than that of the previous clear-sky algorithm. In contrast to the clear-sky algorithm, the all-sky algorithm can easily improve LE estimation at the nonvegetated sites, and maintain the similar accuracy at the vegetated sites. Nonvegetated areas dominate the semi-arid or arid regions and oasis only accounts for certain areas. Therefore, the all-sky algorithm is beneficial to the regional LE estimation in the semiarid/arid region. Considering that the all-sky algorithm can also provide cloudy-sky LE and presents more satisfactory accuracy, this algorithm is a significant improvement relative to previous LE estimation.

Although the all-sky algorithm is efficient, it also has a few shortcomings. In the algorithm, T_s is provided by MYD11 (MYD06) under clear (cloudy) sky. T_s data provided by MYD06 products are derived from the interpolation of the National Centers for Environmental Prediction (NCEP) reanalysis data with coarse spatial resolution. Accordingly, the quality of MYD06 T_s is possibly unsatisfactory in rainy/cloudy days. The accuracy of T_s dominates the accuracy of upwelling longwave radiation, which is the important factor in the estimation of R_n and LE. The qualities of other meteorological factors (T_a, near-surface pressure and the relative humidity) are guaranteed by the ground observations of China Meteorological Administration sites, which are also the input data of CLDAS. Therefore, T_s validation is important to the estimation of R_n and LE. The LE is always retrieved in relatively low accuracy in the rainy/cloudy days. In addition, considering that Δ is computed based on the simplified equation (7) without a linear relationship between the

TABLE V
Errors and Bias of Instantaneous LE Retrieved by All-Sky Algorithm (RSLE) and Clear-Sky Algorithm (MODLE) Under Clear Sky at Six Sites During 25 June to 9 September in 2012

Types	Statistics	Bias	RE	RMSE	R^2
	Unit	W/m^2	%	W/m^2	–
RSLE	Wetland	−96	20	108	0.53
	Vegetable	−111	23	123	0.56
	Orchard	−190	33	199	0.64
	Village	112	39	122	0.56
	Gobi	18	10	106	0.12
	Desert	−28	13	86	0.10
MODLE	Wetland	−69	14	79	0.73
	Vegetable	−50	10	81	0.43
	Orchard	−226	40	245	0.09
	Village	141	49	158	0.29
	Gobi	61	35	116	0.21
	Desert	−93	44	120	0.26

saturation curve between T_s and T_a [16], one of the sources of RSLE error can be ascribed to approximate expression of Δ.

The all-sky algorithm can facilitate further research about temporal upscaling and reconstruction approaches, and daily LE can be obtained by serial instantaneous estimation. The images of geostationary satellites (e.g., Geostationary Operational Environmental Satellite and Fengyun Meteorological Satellite) can offer high-frequency information on the surface and atmosphere per dozens of minutes [60], [61]. Further available and reliable LE estimations can be retrieved by using the all-sky algorithm and these datasets.

VI. Conclusion

On the basis of the NP approach, a clear-sky algorithm of LE using MODIS products was first developed in previous research. To obtain all-sky information, we developed a simple and direct algorithm to estimate LE under all skies using MODIS and CLDAS products, without the need for ground-based meteorological data in this study. The retrieval results were analyzed and validated at six selected sites (vegetated sites: wetland, vegetable, orchard; nonvegetated sites: village, Gobi, desert) within a typical arid/semiarid region (Heihe Basin). The temporal–spatial distribution of RSLE was reliable. At the retrieval moment, RSLE was relatively satisfactory, with bias, R^2, RE, and RMSE values of -59 W/m^2, 0.48, 18%, and 133 W/m^2, respectively. At the site scale, the RSLE was also relatively accurate at all sites, with an R^2 of 0.19–0.63, a bias of -129–57 W/m^2, a RE of 5%–29%, and a RMSE of 95–150 W/m^2. At the nonvegetated sites, the RSLE exhibited relatively good accuracy and poor agreement between the RSLE and ERLE (RE = 5%–23%, R^2 = 0.19–0.40). However, the opposite trend was observed at the vegetated sites (RE = 24%–29%, R^2 = 0.46–0.63). During sunny days, compared with the retrieved LE of the clear-sky algorithm, our all-sky algorithm revealed a more reliable performance at the nonvegetated sites and orchard site, and it also exhibited similar accuracy at the wetland and vegetable sites. For the error source of the retrieved LE, in arid nonvegetated regions, the dominant error contributors (causing 40 W/m^2 of the RSLE error) were R_n, G_s, T_s, and T_a. In the vegetated regions, the input errors were not the dominant error sources of RSLE. Future research should aim to improve the accuracy of LE estimation. In vegetated regions, the systemic underestimation of the NP approach should be addressed. In nonvegetated regions, the quality of MODIS products is expected to improve. Therefore, in the development of the all-sky algorithm, input data and temporal upscaling approach of instantaneous retrieval should be optimized.

Acknowledgment

The authors would like to thank the Cold and Arid Regions Science Data Center at Lanzhou for providing observation data (http://westdc.westgis.ac.cn), the LAADS of NASA for providing MODIS products (http://ladsweb.nascom.nasa.gov), and the National Meteorological Information Center of China for providing CLDAS products (http://data.cma.cn). The authors would also like to thank Prof. S. M. Liu and Dr. Z. W. Xu of the Beijing Normal University for their kind assistance in providing field data and help in field visit.

References

[1] R. Burman and L. O. Pochop, *Evaporation, Evapotranspiration and Climatic Data.* Amsterdam, The Netherlands: Elsevier Science, 1994, p. 278.

[2] T. A. Howell, A. D. Schneider, D. A. Dusek, T. H. Marek, and J. L. Steiner, "Calibration and scale performance of Bushland weighing lysimeters," *Trans. Amer. Soc. Agricutural Eng.*, vol. 38, pp. 1019–1024, 1995.

[3] D. A. Zeweldi, M. Gebremichael, J. Wang, T. Sammis, J. Kleissl, and D. Miller, "Intercomparison of sensible heat flux from large aperture scintillometer and eddy covariance methods: Field experiment over a homogeneous semi-arid region," *Boundary-Layer Meteorol.*, vol. 135, pp. 151–159, 2010.

[4] R. W. Todd, S. R. Evett, and T. A. Howell, "The Bowen ratio-energy balance method for estimating latent heat flux of irrigated alfalfa evaluated in a semi-arid, adjective environment," *Agricultural Forest Meteorol.*, vol. 103, pp. 335–348, 2000.

[5] B. Mueller, S. I. Seneviratne, and C. Jimenez, "Evaluation of global observations-based evapotranspiration datasets and IPCC AR4 simulations," *Geophys. Res. Lett.*, vol. 38, pp. 1–7, 2011.

[6] H. L. Penman, "Natural evaporation from open water, bare soil and grass," *Proc. Roy. Soc. London, A. Math. Phys. Sci.*, vol. 193, no. 1032, pp. 120–145, 1948.

[7] K. R. Knipper, A. M. Kinoshita, and T. S. Hogue, "Evaluation of a moderate resolution imaging spectroradiometer triangle-based algorithm for evapotranspiration estimates in subalpine regions," *J. Appl. Remote Sens.*, vol. 10, no. 1, pp. 016002–016002, 2016.

[8] Z. Su, "The surface energy balance system (SEBS) for estimation of turbulent heat fluxes," *Hydrol. Earth Syst. Sci.*, vol. 6, pp. 85–100, 2002.

[9] Y. Ma, S. Liu, F. Zhang, J. Zhou, Z. Jia, and L. Song, "Estimations of regional surface energy fluxes over heterogeneous oasis–desert surfaces in the middle reaches of the heihe river during HiWATER-MUSOEXE," *IEEE Geosci. Remote Sens. Lett.*, vol. 12, no. 3, pp. 671–675, 2015.

[10] Q. Mu, M. Zhao, and S. W. Running, "Improves to a MODIS global terrestrial evaportranspiration algorithm," *Remote Sens. Environ.*, vol. 115, pp. 1781–1800, 2011.

[11] Y. J. Xiong and G. Y. Qiu, "Estimation of evapotranspiration using remotely sensed land surface temperature and the revised three-temperature model," *Int. J. Remote Sen.*, vol. 32, pp. 5853–5874, 2011.

[12] L. Song *et al.*, "Applications of a thermal-based two-source energy balance model using Priestley-Taylor approach for surface temperature partitioning under advective conditions," *J. Hydrol.*, vol. 540, pp. 574–587, 2016.

[13] R. Dhungel, R. G. Allen, R. Trezza, and C. W. Robison, "Evapotranspiration between satellite overpasses: Methodology and case study in agricultural dominant semi-arid areas," *Meteorological Appl.*, vol. 23, no. 4, pp. 714–730, 2016.

[14] P. D. Colaizzi *et al.*, "Two-source energy balance model estimates of evapotranspiration using component and composite surface temperatures," *Advances Water Resources*, vol. 50, pp. 134–151, 2012.

[15] G. Gan and Y. Gao, "Estimating time series of land surface energy fluxes using optimized two source energy balance schemes: Model formulation, calibration, and validation," *Agricultural Forest Meteorol.*, vol. 208, pp. 62–75, 2015.

[16] R. Dhungel, R. G. Allen, R. Trezza, and C. W. Robison, "Comparison of latent heat flux using aerodynamic methods and using the Penman–Monteith method with satellite-based surface energy balance," *Remote Sens.*, vol. 6, no. 9, pp. 8844–8877, 2014.

[17] Y. Liu, T. Hiyama, T. Yasunari, and H. Tanaka, "A nonparametric approach to estimating terrestrial evaporation: Validation in eddy covariance sites," *Agricultural Forest Meteorol.*, vol. 157, pp. 49–59, 2012.

[18] X. Pan, Y. Liu, and X. Fan, "Satellite retrieval of surface evapotranspiration with nonparametric approach: Accuracy assessment over a semiarid region," *Advances Meteorol.*, vol. 2016, pp. 1584316-1–1584316-14, 2016.

[19] S. Liang, *Quantitative Remote Sensing of Land Surfaces.* New York, NY, USA: Wiley-IEEE Press, 2004, pp. 240–284.

[20] X. Zhao and Y. Liu, "Relative contribution of the topographic influence on the triangle approach for evapotranspiration estimation over mountainous areas," *Advances Meteorol.*, vol. 2014, pp. 584040-1–584040-16, 2014.

[21] S. Liu, H. Su, R. Zhang, J. Tian, S. Chen, and W. Wang, "Regional estimation of remotely sensed evapotranspiration using the surface energy balance-advection (SEB-A) method," *Remote Sens.*, vol. 8, no. 8, pp. 1–14, 2016.

[22] J. Kim and T. Hogue, "Evaluation of a MODIS triangle-based evapotranspiration algorithm for semi-arid regions," *J. Appl. Remote Sens.*, vol. 7, no. 1, pp. 073493–073493, 2013.
[23] K. Knipper, A. Kinoshita, and T. Hogue, "Evaluation of a moderate resolution imaging spectroradiometer triangle-based algorithm for evapotranspiration estimates in subalpine regions," *J. Appl. Remote Sens.*, vol. 10, no. 1, pp. 016002–016002, 2016.
[24] G. Bisht and R. L. Bras, "Estimation of net radiation from the MODIS data under all sky conditions: southern great plains case study," *Remote Sens. Environ.*, vol. 114, no. 7, pp. 1522–1534, 2010.
[25] A. J. Prata, "A new long-wave formula for estimating downward clear-sky radiation at the surface," *Quart. J. Roy. Meteorological Soc.*, vol. 122, pp. 1127–1151, 1996.
[26] M. S. Moran, R. D. Jackson, L. H. Raymond, L. W. Gay, and P. N. Slater, "Mapping surface energy balance components by combining landsat thematic mapper and ground-based meteorological data," *Remote Sens. Environ.*, vol. 30, no. 1, pp. 77–87, 1989.
[27] X. Zhao, "Effects of marshland conversion to cropland on CO_2, H_2O and energy flux in sanjing plain, northeastern china," (in Chinese), Ph.D. thesis, The Institute of Atmospheric Physics, Chinese Academy of Sciences, Beijing, China, 2008.
[28] R. G. Allen, L. S. Pereira, and D. Raes, "Crop Evapotranspiration (guidelines for computing crop water requirements)," FAO Irrigation and Drainage Paper No. 56, Mar. 20, 2015. [Online]. Available: http://www.fao.org/docrep/X0490E/X0490E00.htm
[29] T. Foken, "The energy balance closure problem: An overview," *Ecological Appl.*, vol. 18, no. 6, pp. 1351–1367, 2008.
[30] B. Amiro, "Measuring boreal forest evapotranspiration using the energy balance residual," *J. Hydrol.*, vol. 366, no. 1, pp. 112–118, 2009.
[31] R. G. Allen, L. S. Pereira, T. A. Howell, and M. E. Jensen, "Evapotranspiration information reporting: I. Factors governing measurement accuracy," *Agricultural Water Manage.*, vol. 98, no. 6, pp. 899–920, 2011.
[32] J. R. Nagol, E. F. Vermote, and S. D. Prince, "Effects of atmospheric variation on AVHRR NDVI data," *Remote Sens. Environ.*, vol. 113, pp. 392–397, 2009.
[33] G. L. Squires, *Practical Physics.* Cambridge, U.K.: Cambridge Univ. Press, 2001, pp. 1–41.
[34] E. Kang, G. Cheng, Y. Lan, and H. Jin, "A model for simulating the response of runoff from the mountainous watersheds of inland river basins in the arid area of northwest China to climatic changes," *Sci. China, D, Earth Sci.*, vol. 42, no. 1, pp. 52–63, 1999.
[35] Z. Jia, S. Liu, Z. Xu, Y. Chen, and M. Zhu, "Validation of remotely sensed evapotranspiration over the Hai River Basin, China," *J. Geophys. Res., Atmospheres*, vol. 117, no. D13, pp. 1984–2012, 2012.
[36] X. Li *et al.*, "Heihe watershed allied telemetry experimental research (HiWATER): Scientific objectives and experimental design," *Bull. Amer. Meteorological Soc.*, vol. 94, pp. 1145–1160, 2013.
[37] Z. W. Xu *et al.*, "Intercomparison of surface energy flux measurement systems used during the HiWATER-MUSOEXE," *J. Geophys. Res.*, vol. 118, pp. 13140–13157, 2013.
[38] A. Savtchenko *et al.*, "Terra and Aqua MODIS products available from NASA GES DAAC," *Advances Space Res.*, vol. 34, no. 4, pp. 710–714, 2004.
[39] W. P. Menzel, R. A. Frey, and B. A. Baum, "Cloud top properties and cloud phase—Algorithm theoretical basis document (Collection 006)," 2015. [Online]. Available: http://modis-atmos.gsfc.nasa.gov/_docs/MOD06-ATBD_2015_05_01.pdf
[40] C. H. Dey and L. L. Morone, "Evolution of the national meteorological center global data assimilation system: January 1982-December 1983," *Monthly Weather Rev.*, vol. 113, no. 3, pp. 304–318, 1985.
[41] Z. Wan and J. Dozier, "A generalized split-window algorithm for retrieving land-surface temperature from space," *IEEE Trans. Geosci. Remote Sens.*, vol. 34, no. 4, pp. 892–905, Jul. 1996.
[42] A. Huete, K. Didan, T. Miura, E. P. Rodriguez, X. Gao, and L. G. Ferreira, "Overview of the radiometric and biophysical performance of the MODIS vegetation indices," *Remote Sens. Environ.*, vol. 83, pp. 195–213, 2002.
[43] A. Huete *et al.*, "Amazon rainforests green-up with sunlight in dry season," *Geophys. Res. Lett.*, vol. 33, no. L06405, pp. 1–4, 2006.
[44] C. B. Schaaf *et al.*, "First operational BRDF, albedo nadir reflectance product from MODIS," *Remote Sens. Environ.*, vol. 83, pp. 135–148, 2003.
[45] C. Shi, L. Jiang, T. Zhang, B. Xu, and S. Han, "Status and plans of CMA land data assimilation system (CLDAS) project," *EGU Gen. Assem. Conf. Abstracts*, vol. 16, pp. 1–4, 2014.
[46] W. Gong, "Evaluation on the products of CMA land data assimilation system," (in Chinese), M.D. thesis, Nanjing Univ. Inf. Sci. Technol., Nanjing, China, 2014.
[47] Y. Yamaguchi, A. Kahle, H. Tsu, T. Kawakami, and M. Pniel, "Overview of advanced space-borne thermal emission and reflection radiometer (ASTER)," *IEEE Trans. Geosci. Remote Sens.*, vol. 36, no. 4, pp. 1062–1071, Jul. 1998.
[48] A. Gillespie, S. Rokugawa, T. Matsunaga, S. Cothern, S. Hook, and A. Kahle, "A temperature and emissivity separation algorithm for Advanced Spaceborne Thermal Emission and Reflection Radiometer (ASTER) images," *IEEE Trans. Geosci. Remote Sens.*, vol. 36, no. 4, pp. 1113–1126, Jul. 1998.
[49] H. Li *et al.*, "Evaluation of the VIIRS and MODIS LST products in an arid area of Northwest China," *Remote Sens. Environ.*, vol. 142, pp. 111–121, 2014.
[50] H. Li, H. S. Wang, Y. M. Du, Q. Xiao, and Q. H. Liu, "HiWATER: ASTER LST and LSE dataset in 2012 in the middle reaches of the heihe river basin," Cold Arid Regions Science Data Center at Lanzhou, Lanzhou, China, 2015, doi: 10.3972/hiwater.220.2015.db.
[51] J. Cheng, S. Liang, Y. Yao, and X. Zhang, "Estimating the optimal broadband emissivity spectral range for calculating surface longwave net radiation," *IEEE Geosci. Remote Sens. Lett.*, vol. 10, no. 2, pp. 401–405, Mar. 2013.
[52] S. M. Liu *et al.*, "A comparison of eddy-covariance and large aperture scintillometer measurements with respect to the energy balance closure problem," *Hydrol. Earth Syst. Sci.*, vol. 15, no. 4, pp. 1291–1306, 2011.
[53] S. M. Liu, Z. W. Xu, and W. Z. Wang, "The use of large aperture scintillometer and eddy covariance system for monitoring energy and water vapor fluxes over different surfaces in the Heihe river basin, China," *IAHS-AISH Publication*, pp. 184–190, 2012.
[54] Z. Xu, Y. Ma, S. Liu, W. Shi, and J. Wang, "Assessment of the energy balance closure under advective conditions and its impact using remote sensing data," *J. Appl. Meteorol. Climatol.*, vol. 56, pp. 127–140, 2017.
[55] S. Liu *et al.*, "Upscaling evapotranspiration measurements from multi-site to the satellite pixel scale over heterogeneous land surfaces," *Agricultural Forest Meteorol.*, vol. 230–231, pp. 97–113, 2017.
[56] Z. L. Li *et al.*, "A review of current methodologies for regional evapotranspiration estimation from remotely sensed data," *Sensors*, vol. 9, no. 5, pp. 3801–3853, 2009.
[57] G. L. Tian, Q. H. Liu, and L. Chen, *Thermal Remote Sensing*. Beijing, China: Publishing House of Electronics Industry, 2006.
[58] Y. Liu, G. Wu, and C. Ke, *Hydrological Remote Sensing*. Beijing, China: Publishing House of Science, 2016.
[59] T. Xu, S. Liu, L. Xu, Y. Chen, Z. Jia Z. Xu, and J. Nielso, "Temporal upscaling and reconstruction of thermal remotely sensed instantaneous evapotranspiration," *Remote Sens.*, vol. 7, no. 3, pp. 3400–3425, 2015.
[60] D. Sun and R. T. Pinker, "Estimation of land surface temperature from a geostationary operational environmental satellite (GOES-8)," *J. Geophys. Res., Atmospheres*, vol. 108, no. D11, pp. 1–15, 2003.
[61] B. Tang, Y. Bi, Z. Li, and J. Xia, "Generalized split-window algorithm for estimate of land surface temperature from Chinese geostationary FengYun meteorological satellite (FY-2C) data," *Sensors*, vol. 8, no. 2, pp. 933–951, 2008.

Xin Pan received the B.S. degree in surveying and mapping from Wuhan University, Wuhan, China, in 2011, the M.S. degree in surveying and mapping from Hohai University, Nanjing, China, in 2013, and the Ph.D. degree in cartography and geographical information system from the Nanjing Institute of Geography and Limnology, Chinese Academy of Sciences, Nanjing, in 2016.

He is currently a Postdoctoral Teacher with the School of Earth Science and Engineering, Hohai University. His research interests include the remote sensing retrieval and validation of land surface evapotranspiration and net radiation.

Yuanbo Liu received the M.S. degree in physical geography from the Lanzhou Institute of Desert Research, Chinese Academy of Sciences, Lanzhou, China, in 1994 and the Ph.D. degree in bioenvironmental sciences from Tottori University, Tottori, Japan, in 2003.

He is currently a Professor of satellite hydrology with the Nanjing Institute of Geography and Limnology, Chinese Academy of Sciences, Nanjing, China. His research interests include quantitative remote sensing and hydrology.

Guojing Gan received the B.S. degree in hydraulic and hydro-power engineering in 2010 from Tsinghua University, Beijing, China, and the Ph.D. degree in physical geography in 2016 from the Institute of Geographic Science and Nature Resources Research, Chinese Academy of Sciences, Beijing.

He is currently an Assistant Professor with the Nanjing Institute of Geography and Limnology, Chinese Academy of Sciences. His scientific interests include the remote sensing retrieval and validation of land surface evapotranspiration.

Xingwang Fan received the B.S. degree in surveying and mapping and the M.S. degree in photogrammetry and remote sensing from Southeast University, Nanjing, China, in 2009 and 2012, and the Ph.D. degree in cartography and geographical information system from the Nanjing Institute of Geography and Limnology, Chinese Academy of Sciences, Nanjing, in 2015.

He is currently an Assistant Professor with the Nanjing Institute of Geography and Limnology, Chinese Academy of Sciences. His scientific interests include satellite data consistency and uncertainties in remote sensing.

Yingbao Yang received the Ph.D. degree in cartography and geographical information system from the Nanjing Institute of Geography and Limnology, Chinese Academy of Sciences, Nanjing, China, in 2005.

She is currently an Associate Professor with School of Earth Science and Engineering, Hohai University, Nanjing. Her scientific interests include the remote sensing retrieval of land surface temperature and the analysis of urban thermal environment.